Eur. Phys. J. C 7, 643–654 (1999)
DOI 10.1007/s100529801035

THE EUROPEAN PHYSICAL JOURNAL C

The description of F_2 at low Q^2

A.D. Martin[1], M.G. Ryskin[1,2], A.M. Stasto[1,3]

[1] Department of Physics, University of Durham, Durham, DH1 3LE, UK
[2] Petersburg Nuclear Physics Institute, 188350, Gatchina, St. Petersburg, Russia
[3] H. Niewodniczanski Institute of Nuclear Physics, 31-342 Krakow, Poland

Received: 1 June 1998 / Revised version: 4 September 1998 / Published online: 19 November 1998

Abstract. We analyse the data for the proton structure function F_2 over the entire Q^2 domain, including especially low Q^2, in terms of perturbative and non-perturbative QCD contributions. The small distance configurations are given by perturbative QCD, while the large distance contributions are given by the vector dominance model and, for the higher mass $q\bar{q}$ states, by the additive quark approach. The interference between states of different $q\bar{q}$ mass (in the perturbative contribution) is found to play a crucial role in obtaining an excellent description of the data throughout the whole Q^2 region, including photoproduction.

1 Introduction

There now exist high precision deep inelastic ep scattering data [1,2] covering both the low Q^2 and high Q^2 domains, as well as measurements of the photoproduction cross section. The interesting structure of these measurements, in particular the change in the behaviour of the cross section with Q^2 at $Q^2 \sim 0.2\text{GeV}^2$, highlight the importance of obtaining a theoretical QCD description which smoothly links the non-perturbative and perturbative domains.

In any QCD description of a $\gamma^* p$ collision, the first step is the conversion of the initial photon into a $q\bar{q}$ pair, which is then followed by the interaction of the pair with the target proton. Let $\sigma(s, Q^2)$ be the total cross section for the process $\gamma^* p \to X$ where Q^2 is the virtuality of the photon and $\sqrt{s}$ is the $\gamma^* p$ centre-of-mass energy. It is related to the forward $\gamma^* p$ elastic amplitude A by the optical theorem, $\text{Im}\ A = s\sigma$. We may write a double dispersion relation [3] for A and obtain for fixed s

$$\sigma(s,Q^2) = \sum_q \int \frac{dM^2}{M^2+Q^2} \int \frac{dM'^2}{M'^2+Q^2}\, \rho(s,M^2,M'^2) \times \frac{1}{s}\,\text{Im}\, A_{q\bar{q}+p}(s,M^2,M'^2) \qquad (1)$$

where M and M' are the invariant masses of the incoming and outgoing $q\bar{q}$ pair. The relation is shown schematically in Fig. 1. If we assume that forward $q\bar{q}+p$ scattering does not change the momentum of the quarks[1] then $A_{q\bar{q}+p}$ is proportional to $\delta(M^2 - M'^2)$, and (1) becomes

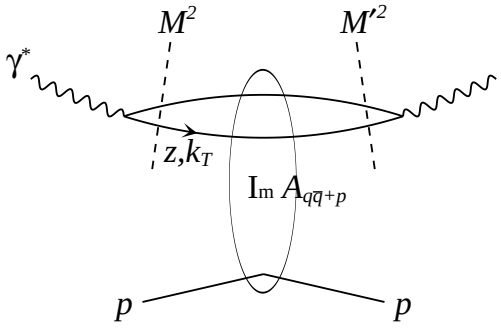

Fig. 1. The schematic representation of the double dispersion (1) for the $\gamma^* p$ total cross section $\sigma(s, Q^2)$ at fixed c.m. energy $\sqrt{s}$. The cut variables, M and M', are the invariant masses of the incoming and outgoing $q\bar{q}$ states in the quasi-elastic forward amplitude, $A_{q\bar{q}+p}$

$$\sigma(s,Q^2) = \sum_q \int_0^\infty \frac{dM^2}{(M^2+Q^2)^2}\, \rho(s,M^2) \times \sigma_{q\bar{q}+p}(s,M^2) \qquad (2)$$

where the spectral function $\rho(s, M^2)$ is the density of $q\bar{q}$ states.

Following Badelek and Kwiecinski [4] we may divide the integral into two parts[2], the region $M^2 < Q_0^2$ described by the vector meson dominance model (VDM) and the region $M^2 > Q_0^2$ described by perturbative QCD. Suppose that we assume $\rho\sigma_{q\bar{q}+p}$ is a constant independent of M^2

[1] In a more detailed treatment this assumption is no longer valid, see (22) and (29) below, and the discussion in Sect. 4

[2] Although Badelek and Kwiecinski base their fit to the data on (2), they also discuss the more general case in which $M \neq M'$ contributions may be included in the spectral function ρ

(which should be true modulo logarithmic QCD corrections) then the perturbative component of the integral is

$$\int_{Q_0^2}^{\infty} \frac{dM^2}{(M^2+Q^2)^2}\,\rho\sigma = \int_0^{\infty} \frac{dM^2}{(M^2+Q^2+Q_0^2)^2}\,\rho\sigma = \sigma(s, Q^2+Q_0^2). \quad (3)$$

Thus (2) becomes

$$\sigma(s,Q^2) \;=\; \sigma(\mathrm{VDM}) + \sigma^{\mathrm{QCD}}\,(s, Q^2+Q_0^2) \quad (4)$$

where the QCD superscript indicates that the last contribution is to be calculated entirely from perturbative QCD.

We may use

$$\sigma(s,Q^2) \;=\; \frac{4\pi^2\alpha}{Q^2}\,F_2(x,Q^2) \quad (5)$$

where $x = Q^2/(s+Q^2-M^2)$ to rewrite (4) as

$$F_2(x,Q^2) \;=\; F_2(\mathrm{VDM}) + \frac{Q^2}{Q^2+Q_0^2} F_2^{\mathrm{QCD}}(\overline{x}, Q^2+Q_0^2) \quad (6)$$

where $\overline{x} = (Q^2+Q_0^2)/(s+Q^2+Q_0^2-M^2)$. The vector meson dominance term has the form[3]

$$F_2(\mathrm{VDM}) \;=\; \frac{Q^2}{4\pi} \sum_V \frac{M_V^4\,\sigma_V\,(s)}{\gamma_V^2 (Q^2+M_V^2)^2} \quad (7)$$

where M_V is the mass of vector meson V and where the sum is over the vector mesons which fall in the region $M_V^2 < Q_0^2$. The vector meson-proton cross sections $\sigma_V(s)$ can be determined from the πp and Kp total cross sections using the additive quark model and γ_V^2 from the leptonic width of the vector meson V. The last term in (6) can be determined from perturbative QCD using the known parton distributions. This approach was first proposed by Badelek and Kwiecinski (BK) [4]. We see that the BK model, (4) and (6), makes a parameter free prediction of $F_2(x,Q^2)$ which is expected to be valid, for $s \gg Q^2$, for all Q^2 including very low Q^2. The BK predictions give an excellent description of the F_2 data for $Q^2 \gtrsim 1$ GeV^2, but overshoot the new measurements of F_2 for smaller values of Q^2. This deficiency of the model was removed in a fit to the F_2 data performed by the H1 collaboration [1], but at the expense of using an unreasonably low value for $Q_0^2 = 0.45\mathrm{GeV}^2$ and of introducing an ad hoc factor of 0.77 to suppress the VDM term.

The Badelek-Kwiecinski idea to separate perturbative and non-perturbative contributions is very attractive. To exploit it further we must achieve a better separation between the short and long distance contributions. To do this we take a two-dimensional integral over the longitudinal and transverse momentum components of the quark, rather than simply over the mass M of the $q\overline{q}$ pair.

The contribution coming from the small mass region is pure VDM and is given by (7). However, the behaviour of the cross section at large M^2 is a more delicate question. The part which comes from large k_T of the quark can be calculated by perturbative QCD in terms of the known parton distributions, whereas for small k_T we will use the additive quark model and the impulse approximation. That is only one quark interacts with the target and the quark-proton cross section is well approximated by one third of the proton-proton cross section.

At this point it is interesting to note some recent excellent parametric fits of the low Q^2 data for F_2, or rather for $\sigma(\gamma^* p)$; see Sect. 8 of [5] for a recent review. One fit is based on (2) and the generalised VDM [6]. To be more precise it is based entirely on a parametrization of the vector meson + proton cross section and does not take advantage of our present knowledge of perturbative QCD. As a consequence some anomalies appear. For instance the photoproduction cross section becomes negative for $\sqrt{s} < 6$GeV (or $\sigma(Vp) < 0$ for $M_V > 0.26\sqrt{s}$). Second the model has anomalously large values of $R = \sigma_L/\sigma_T$ (where F_L is obtained by including a factor $\xi Q^2/M_V^2$ on the right-hand-side of formula (7) for F_T). In the well-known deep inelastic region the model predicts $R > 1$ for $Q^2 > 35\mathrm{GeV}^2$ and $x > 0.01$ (and even $R > 4$ for $x > 0.1$) whereas the data indicate that $R \simeq 0.2 - 0.3$. This effect probably reflects, as the authors note, the omission of allowing ξ to depend on Q^2, see (32) below. Rather their model has $\xi = 0.171$ for all Q^2.

An earlier approach based on the generalised VDM can be found in [7]. In addition to the VDM contributions, this work contains a contribution at small x coming from "heavy" long-lived fluctuations of the incoming photon, which are parametrized in terms of a "hard" Pomeron whose intercept is found to be $\alpha_{P'} = 1.289$.

An excellent fit to the data has also been obtained in [8] by assuming that perturbative QCD evolution is applicable to the lowest values of Q^2, using both a hard (singular) input form, $x^{-0.47}$, together with a soft (constant) Pomeron term. The latter term is modified by a factor $Q^2/(Q^2+M^2)$ with $M = 0.87$ GeV and, moreover is assumed not to evolve at low Q^2. In order to achieve a finite cross section as $Q^2 \to 0$, the model assumes that the strong coupling α_S saturates and requires the two remaining perturbative terms (the hard singlet term and a non-singular, non-singlet contribution) to vanish as $Q^2 \to 0$. The model is thus quite contrived, but this is the price to be paid when using perturbative QCD in a domain in which it is not applicable.

There have been a number of Regge-motivated models in which the Pomeron intercept is allowed to vary with Q^2, see for example [9] and [10]. The idea is that at low Q^2 we see a "shadowed" rather than a "bare" Pomeron, then as Q^2 increases the shadowing effects disappear to reveal a hard Pomeron with a larger intercept. The early models do not reproduce the new low Q^2 data, but a very recent phenomenological fit along these lines shows that a good description is possible [11]. Another recent fit, based on the Regge motivated ALLM parametrization [10], can be found in [12]. The description, with 23 parameters, describes the data well and may be used to interpolate the

[3] Strictly speaking (7) is the formula F_T. The small longitudinal component will be discussed later

measurements. On the other hand the physical basis of the parametrization is not clear. For example a variable $x_{I\!P}$ is defined by

$$\frac{1}{x_{I\!P}} \;=\; 1 \;+\; \frac{W^2 - M^2}{Q^2 + M^2_{I\!P}} \tag{8}$$

where $W = \sqrt{s}$ is the $\gamma^* p$ centre-of-mass energy, M is the proton mass and $M_{I\!P}$ reflects the energy scale of Pomeron exchange. This latter scale turns out to be extremely large, $M^2_{I\!P} = 49.5$ GeV^2, much larger than any hadron or glueball mass. Secondly the intercept, $\alpha_R(0)$, of the secondary trajectory decreases with Q^2, which is contrary to Regge theory (where α_R is independent of Q^2).

The description of the F_2 or $\sigma(\gamma^* p)$ data presented in this paper is quite different. We use a physically motivated approach with very few free parameters, and we clearly separate the contributions to F_2 coming from the large (small quark k_T) and small (large k_T) distances. A recent study with a similar philosophy to ours can be found in [13]. They achieve a qualitative description of the experimental data over a wide range of photon virtualities (Q^2) and energies (W) in terms of short and long distance contributions. They emphasize that even in the very low Q^2 region the short distance contribution is not small, and also that at large Q^2 the long distance effects still contribute. Here we present a quantitative study which involves a more precise approximation for the $q\bar{q}+p$ cross section and includes consideration of the longitudinal structure function F_L. Other differences are that we compute the (small k_T) non-perturbative component using the VDM for small $q\bar{q}$ masses $M < Q_0$ and the additive quark model for $M > Q_0$; we do not need an artificial suppression[4] of the VDM component. Moreover we make a careful treatment of the perturbative component, repeating the entire analysis of [14], which involves solving coupled integro-differential equations for the gluon-quark singlet distributions. This method means that we are working directly in terms of an unintegrated gluon distribution $f(x, k_T^2)$, which satisfies a unified evolution equation that embodies both DGLAP and BFKL evolution. It has the advantage that it is applicable over the entire perturbative domain since it performs the resummation of both leading $\log(1/x)$ and $\log(Q^2)$ terms.

2 The $\gamma^* p$ cross section

The spectral function ρ occurring in (1) may be expressed in terms of the $\gamma^* \to q\bar{q}$ matrix element $\mathcal{M}$. We have $\rho \propto |\mathcal{M}|^2$ with, for transversely polarised photons,

$$\begin{aligned}\mathcal{M}_T &= \frac{\sqrt{z(1-z)}}{\overline{Q}^2 + k_T^2} \quad \overline{u}_\lambda (\gamma \cdot \varepsilon_\pm) u_{\lambda'} \\ &= \frac{(\varepsilon_\pm \cdot k_T)[(1-2z)\lambda \mp 1]\, \delta_{\lambda,-\lambda'} \;+\; \lambda m_q\, \delta_{\lambda\lambda'}}{\overline{Q}^2 + k_T^2}.\end{aligned} \tag{9}$$

[4] In [13] an ad hoc suppression factor of 0.6 is used

We use the notation of [15], which was based on the earlier work of [16]. Namely the photon polarisation vectors are

$$\varepsilon_T \;=\; \varepsilon_\pm \;=\; \frac{1}{\sqrt{2}}\,(0,\, 0,\, 1,\, \pm i), \tag{10}$$

and $\lambda, \lambda' = \pm 1$ corresponding to $q, \bar{q}$ helicities of $\pm\frac{1}{2}$. Also we introduce

$$\overline{Q}^2 \;=\; z(1-z)Q^2 + m_q^2. \tag{11}$$

Note that (9) is written in terms of "old-fashioned" time-ordered or light cone perturbation theory where both the q and $\bar{q}$ are on-mass-shell. This form is appropriate when discussing the dispersion relation (1) in the $q\bar{q}$ invariant mass. For high photon momentum p_γ the two time-ordered diagrams have a very different energy mismatch

$$\left(\Delta E \;\simeq\; \frac{Q^2 + M^2}{2p_\gamma}\right) \;\ll\; (\Delta E' \;\simeq\; p_\gamma)\,, \tag{12}$$

and so the contribution from the diagram ($\Delta E'$) with the "wrong" time-ordering may be neglected. The remaining diagram, with energy denominator $1/\Delta E$, leads to the behaviour $1/(\bar{Q}^2 + k_T^2)$ contained in (9), as can be seen on using (14) below.

In terms of the quark momentum variables z, k_T^2 of Fig. 1, (1) and (2) become

$$\begin{aligned}\sigma_T &= \sum_q \alpha \frac{e_q^2}{4\pi^2} \sum_{\lambda\,=\,\pm\,1} \int dz\, d^2k_T\, (\mathcal{M}_T \mathcal{M}_T^*) N_c \\ &\quad \times \frac{1}{s}\, \mathrm{Im}\, A_{q\bar{q}+p} \\ &= \sum_q \alpha \frac{e_q^2}{2\pi} \int dz\, dk_T^2 \frac{[z^2 + (1-z)^2]k_T^2 + m_q^2}{(\overline{Q}^2 + k_T^2)^2} \\ &\quad \times N_c\, \sigma_{q\bar{q}+p}(k_T^2)\end{aligned} \tag{13}$$

where the number of colours $N_c = 3$, and e_q is the charge of the quark in units of e. We shall give the corresponding cross section σ_L for longitudinal polarised photons in Sect. 2.1.

The dispersion relation (2) in M^2 has become, in (13), a two dimensional integral. The relation between the variables is

$$M^2 \;=\; \frac{k_T^2 + m_q^2}{z(1-z)} \tag{14}$$

where m_q is the mass of the quark. For massless quarks $z = \frac{1}{2}(1 + \cos\theta)$, where θ is the angle of the outgoing quark with respect to the photon in the $q\bar{q}$ rest frame. The dz integration is implicit in (2) as the integration over the quark angular distribution in the spectral function ρ.

To determine $F_2(x, Q^2)$ at low Q^2 we have to evaluate the contributions to σ_T coming from the various kinematic domains. First the contribution from the perturbative domain with $M^2 > Q_0^2$ and large k_T^2, and second from the non-perturbative or long-distance domains.

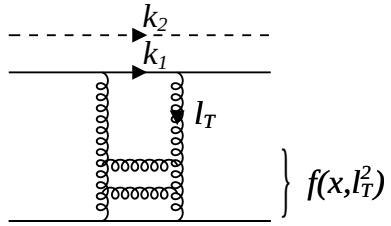

Fig. 2. The quark-proton interaction via two gluon exchange. The spectator (anti)quark is shown by the dashed line. $f(x, l_T^2)$ is the unintegrated gluon distribution of the proton

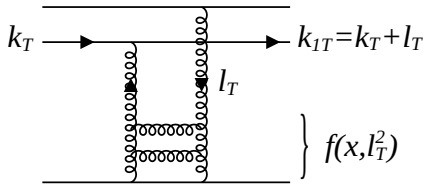

Fig. 3. A "non-diagonal" $q\bar{q}-$ proton interaction

2.1 The $\gamma^* p$ cross section in the perturbative domain

We may begin with the two gluon exchange contribution to quark–quark scattering

$$\sigma_{q+q} \;=\; \frac{2}{9}\,4\pi\,\int \alpha_S^2(l_T^2)\,\frac{dl_T^2}{l_T^4} \tag{15}$$

where $\pm\boldsymbol{l}_T$ are the transverse momenta of the gluons. Thus for q-proton scattering we obtain

$$\sigma_{q+p} \;=\; \frac{2}{3}\,\pi^2\int \alpha_S(l_T^2)\,f(x,l_T^2)\,\frac{dl_T^2}{l_T^4} \tag{16}$$

where

$$f(x,l_T^2) = x\partial g(x,l_T^2)/\partial \ln l_T^2 \tag{17}$$

is the unintegrated gluon density. The process is shown in Fig. 2. Finally for $q\bar{q}+$ proton scattering we have to include the graph for $\bar{q}+p$ scattering. For both the q and $\bar{q}$ interactions we have two diagrams of the type shown in Fig. 3 with $\mathcal{M}^*(\boldsymbol{k}_T+\boldsymbol{l}_T)$ and $\mathcal{M}(k_T)$. We obtain

$$\sigma_T = \sum_q \frac{\alpha e_q^2}{\pi}\int d^2k_{1T}\,dz\,d^2l_T\,\frac{f(x,l_T^2)}{l_T^4}\,\alpha_S(l_T^2) \times\left\{\left[(1-z)^2+z^2\right]\left(\frac{\boldsymbol{k}_{1T}}{D_1}+\frac{\boldsymbol{l}_T-\boldsymbol{k}_{1T}}{D_2}\right)^2 + m_q^2\left(\frac{1}{D_1}-\frac{1}{D_2}\right)^2\right\} \tag{18}$$

where

$$x \;=\; (Q^2+M^2)/s, \tag{19}$$

$$D_1 = k_{1T}^2 \;+\; z(1-z)Q^2 \;+\; m_q^2,$$
$$D_2 = (\boldsymbol{l}_T-\boldsymbol{k}_{1T})^2 \;+\; z(1-z)Q^2 \;+\; m_q^2. \tag{20}$$

Expression (18) is written as the square of the amplitude for quark-antiquark production, where we integrate over the quark momentum k_{1T} in the inelastic *intermediate* state, see Fig. 2. The first term, proportional to $1/D_1$, corresponds to the amplitude where the gluon couples to the antiquark k_2, while in the second term, proportional to $1/D_2$, the gluon couples to the quark k_1. Of course form (18) can also be used to calculate the cross section for high k_T dijet production ($\gamma^* p \to q\bar{q}p$), where k_{1T} and k_{2T} refer to the transverse momenta of the *outgoing* quark jets.

To separate the perturbative and non-perturbative contributions to the cross section (18) for our inclusive process we have to introduce a cut on the quark transverse momentum (as well as on the $q\bar{q}$ invariant mass M). At first sight it might appear that to obtain the perturbative contribution we simply require $k_{1T} > k_0$. However this implementation of the cut-off would not be correct. For instance if, as in Fig. 2, the two exchanged gluons couple to the k_1 line, then $\boldsymbol{k}_{2T} = \boldsymbol{l}_T - \boldsymbol{k}_{1T}$ may be small and in the limit $m_q \to 0$ and small Q^2 we would have an unphysical infrared singularity in the region of large k_{1T} and l_T, but small k_{2T}, coming from the $1/D_2$ term in (18). To see better the origin of the infrared singularities we perform the square and write the expression in curly brackets in (18) in the form

$$\left\{\frac{[(1-z)^2+z^2]k_{1T}^2+m_q^2}{D_1^2} + \frac{[(1-z)^2+z^2](\boldsymbol{l}_T-\boldsymbol{k}_{1T})^2+m_q^2}{D_2^2} + 2\frac{[(1-z)^2+z^2]\boldsymbol{k}_{1T}\cdot(\boldsymbol{l}_T-\boldsymbol{k}_{1T})-m_q^2}{D_1D_2}\right\}. \tag{21}$$

The danger comes from the second term, which corresponds to Fig. 2, whereas the last term, which describes interference, is infrared stable, as we will show later. Our aim is to separate off all the infrared contributions into the non-perturbative part. Therefore to evaluate the perturbative contribution coming from the second term we have to use the cut-off $|\boldsymbol{l}_T - \boldsymbol{k}_{1T}| > k_0$. This is equivalent to changing the variable of integration for the second term from $\boldsymbol{k}_{1T}$ to $\boldsymbol{l}_T - \boldsymbol{k}_{1T}$, and so its contribution is exactly equal to that of the first term. An alternative way to introduce the same cut-off is to separate off the incoming $q\bar{q}$ configurations with $k_T < k_0$ so that (18) becomes

$$\sigma_T = \sum_q \frac{2\alpha e_q^2}{\pi}\int_{k_0^2} d^2k_T dz d^2l_T\,\frac{f(x,l_T^2)}{l_T^4}\,\alpha_S(l_T^2) \times\left\{\frac{[(1-z)^2+z^2]k_T^2+m_q^2}{(\bar{Q}^2+k_T^2)^2} - \frac{[(1-z)^2+z^2]\boldsymbol{k}_T\cdot(\boldsymbol{k}_T+\boldsymbol{l}_T)+m_q^2}{(\bar{Q}^2+k_T^2)(\bar{Q}^2+(\boldsymbol{k}_T+\boldsymbol{l}_T)^2)}\right\}. \tag{22}$$

Note that the transverse momentum $\boldsymbol{k}_T$ of the incoming quark is equal to $\boldsymbol{k}_{1T}$ when the gluon couples to the antiquark (first term in (21)) and is equal to $\boldsymbol{k}_{1T}-\boldsymbol{l}_T$ when the

gluon couples to the quark (second term in (21)). Working in terms of the variable $\boldsymbol{k}_T$ corresponding to the dispersion cut shown in F ig. 1 has the advantage that it is then easy to introduce cut-offs with respect to the invariant $q\bar{q}$ masses M and M', which we need to impose in order to separate off the non-perturbative VDM contribution[5].

Another argument in the favour of the cut written in terms of initial quark momenta k_T comes from the impact parameter representation. Instead of k_T we may use the transverse coordinate b and write the cross section (22) in the form

$$\sigma_T \ \propto \ \int dz d^2b |\Psi_\gamma(b)|^2 f(x,b) \alpha_S(b) \tag{23}$$

where the gluon distribution

$$f(x,b) \ = \ \int \frac{d^2 l_T}{(2\pi)^2} [1 - e^{i\boldsymbol{l}_T \cdot \boldsymbol{b}}] \frac{f(x,l_T^2)}{l_T^4}. \tag{24}$$

The photon "wave function" is given by [17]

$$|\Psi_\gamma(b)|^2 \ = \ \sum_q \alpha e_q^2 [z^2 + (1-z)^2] \bar{Q}^2 K_1^2(\bar{Q}b), \tag{25}$$

where for simplicity we have set $m_q = 0$. The photon wave function is simply the Fourier transform of the matrix element $\mathcal{M}$ given by (9). It is most natural to take the infrared cut-off in coordinate space, say $b < b_0$. The variable which is the Fourier conjugate of b is the *incoming* quark momentum k_T of Fig. 1 (rather than the *intermediate* transverse momentum k_{1T} of Fig. 2). This is further justification to impose the infrared cut in the form $k_T > k_0$.

Now let us consider the interference contribution, that is the last term in (22). It is infrared stable since in the limit $m_q^2 \to 0$ and $Q^2 \to 0$ it takes the form

$$\int \frac{d^2 k_T \boldsymbol{k}_T \cdot (\boldsymbol{k}_T + \boldsymbol{l}_T)}{k_T^2 (\boldsymbol{k}_T + \boldsymbol{l}_T)^2} \ \sim \ \int \frac{d(|\boldsymbol{k}_T + \boldsymbol{l}_T|)}{k_T} \tag{26}$$

when $|\boldsymbol{k}_T + \boldsymbol{l}_T|$ is small. We have used boundaries $k_T^2 = k_0^2$ and $M^2 = Q_0^2$ to separate the perturbative QCD (pQCD), additive quark model (AQM) and vector meson dominance (VDM) contributions. As a result the $\gamma^* p$ cross section formulae, (22), is asymmetric between the ingoing and outgoing quarks. The origin of the asymmetry is the difference of the transverse momentum of the outgoing quark $(\boldsymbol{k}_T + \boldsymbol{l}_T)$ and the incoming quark $(\boldsymbol{k}_T)$ in Fig. 3. Such a graph therefore represents the interference between M and $M' \neq M$ states. To obtain the pure pQCD contribution we require the incoming $q\bar{q}$ system to satisfy $M^2 > Q_0^2$ and $k_T > k_0$. Ideally we would like to impose the same cuts on the outgoing $q\bar{q}$ system, namely

$$M'^2 \ = \ \frac{(\boldsymbol{k}_T + \boldsymbol{l}_T)^2 \ + \ m_q^2}{z(1-z)} \ > \ Q_0^2 \tag{27}$$

and $k'_T = |\boldsymbol{k}_T + \boldsymbol{l}_T| > k_0$. However in a small region of phase space, where $\boldsymbol{l}_T$ lies close to $-\boldsymbol{k}_T$, we may have $M' < Q_0$ and/or $k'_T < k_0$. For this region we therefore have interference between the pQCD and VDM (or AQM) contributions. There is no double counting since neither our VDM or AQM[6] components contain interference terms. This is fortunate because we cannot neglect the contribution from this small part of phase space of Fig. 3 without destroying gauge invariance, which is provided by the sum of the graphs in Figs. 2 and 3. We stress that the contribution coming from this limited region $\boldsymbol{l}_T$ close to $-\boldsymbol{k}_T$ is infrared stable and hence it is small and has little impact on the overall fit to the data.

So far we have only calculated σ_T. In the same way we may calculate the cross section for longitudinally polarised incident photons. In this case the relation analogous to (13) reads

$$\sigma_L = \sum_q \frac{\alpha e_q^2}{2\pi} \int dz dk_T^2 \ \frac{4Q^2 \, z^2 (1-z)^2 N_c}{(\overline{Q}^2 + k_T^2)^2} \times \sigma_{q\bar{q}+p}(k_T^2), \tag{28}$$

which on evaluating $\sigma_{q\bar{q}+p}$ gives

$$\sigma_L = \sum_q \frac{2\alpha e_q^2}{\pi} \, Q^2 \int_{k_0^2} d^2 k_T dz \, d^2 l_T \ \frac{f(x,l_T^2)}{l_T^4} \times \alpha_S(l_T^2) 4 z^2 (1-z)^2 \ \left\{ \frac{1}{(\bar{Q}^2 + k_T^2)^2} - \frac{1}{(\bar{Q}^2 + k_T^2)(\bar{Q}^2 + (\boldsymbol{k}_T + \boldsymbol{l}_T)^2)} \right\}. \tag{29}$$

From the formal point of view the integrals over l_T^2 and k_T^2 cover the interval 0 to ∞. For the l_T^2 integration in the domain $l_T^2 < l_0^2 \sim 1\text{GeV}^2$ we may use the approximation

$$\alpha_S(l_T^2) \, f(x,l_T^2) \ = \ \frac{l_T^2}{l_0^2} \, \alpha_S(l_0^2) \, f(x,l_0^2). \tag{30}$$

For $k_T^2 < k_0^2$ we enter the long distance domain which we discuss next. To be precise we use the formula (22) and (29) to evaluate the cross sections only in the perturbative domain $M^2 > Q_0^2$ and $k_T^2 > k_0^2$. We exclude the region $M^2 < Q_0^2$ and $k_T^2 > k_0^2$ from the perturbative domain as the point-like (short-distance) component of the vector meson wave function will be included in the VDM term.

2.2 The $\gamma^* p$ cross section in the non-perturbative domain

There are two different non-perturbative contributions. First for $M^2 < Q_0^2$ we use the conventional vector meson dominance formula (7) for $F_T(x,Q^2)$. We also should include the longitudinal structure function $F_L(x,Q^2)$. F_L

[5] Of course the use of the Feynman rules would yield the same result, but the time-ordered or light cone approach with the incoming q and $\bar{q}$ on-shell is more convenient when we come to separate off the non-perturbative component in terms of $k_T < k_0$ and $M, M' < Q_0$

[6] For the AQM contribution the interaction with the target proton is described by the forward elastic quark scattering amplitude and hence we have $z' = z$, $k'_T = k_T$ and $M = M'$

is given by a formula just like (7) but with the introduction of an extra factor $\xi Q^2/M_V^2$ on the right-hand side. $\xi(Q^2)$ is a phenomenological function which should decrease with increasing Q^2. The data for ρ production indicate that $\xi(m_\rho^2) \lesssim 0.7$ [18], whereas at large Q^2 the usual properties of deep inelastic scattering predict that

$$\frac{F_L}{F_T} \sim \frac{4k_T^2}{Q^2} \lesssim \frac{M_V^2}{Q^2}. \tag{31}$$

So throughout the whole Q^2 region the contribution of F_L is less than that of F_T. In order to calculate F_L (VDM) we insert the factor $\xi Q^2/M_V^2$ in (7) and use an interpolating formula for ξ

$$\xi = \xi_0 \left(\frac{M_V^2}{M_V^2+Q^2}\right)^2 \tag{32}$$

with $\xi_0 = 0.7$, which accommodates both the ρ meson results and the deep inelastic expectations of (31). However the recent ρ electroproduction, $\gamma^* p \to \rho p$, measurements [19] indicate that $\sigma_L(\rho)/\sigma_T(\rho)$ may tend to a constant value for large Q^2. We therefore also show the effect of calculating F_L (VDM) from (7) using

$$\xi = \xi_0 \left(\frac{M_V^2}{M_V^2+Q^2}\right), \tag{33}$$

see Fig. 9 below.

The second non-perturbative contribution covers the low k_T part of the $M^2 > Q_0^2$ domain, that is the region with $k_T^2 < k_0^2$. Here we use the additive quark model and the impulse approximation to evaluate the $\sigma_{q\bar{q}+p}$ cross sections in formulas (13) and (28).

2.3 Final formulae

For completeness we list below the formulae that we use for the non-pQCD contributions coming from the $k_T < k_0$ domain. When $M < Q_0$, with $Q_0^2 \simeq 1 - 1.5\text{GeV}^2$, we use the vector meson dominance model. We have

$$\sigma_T(\text{VDM}) = \pi\alpha \sum_{V=\rho,\omega,\phi} \frac{M_V^4\, \sigma_V(W^2)}{\gamma_V^2 (Q^2+M_V^2)^2} \tag{34}$$

$$\sigma_L(\text{VDM}) = \pi\alpha \sum_{V=\rho,\omega,\phi} \frac{Q^2 M_V^2\, \sigma_V(W^2)}{\gamma_V^2 (Q^2+M_V^2)^2}\, \xi_0 \times \left(\frac{M_V^2}{Q^2+M_V^2}\right)^2 \tag{35}$$

with $\xi_0 = 0.7$, see (32). For the vector meson-proton cross sections, we take

$$\begin{aligned} \sigma_\rho = \sigma_\omega &= \tfrac{1}{2}\left[\sigma(\pi^+ p) + \sigma(\pi^- p)\right] \\ \sigma_\phi &= \sigma(K^+ p) + \sigma(K^- p) - \tfrac{1}{2}\left[\sigma(\pi^+ p) + \sigma(\pi^- p)\right]. \end{aligned} \tag{36}$$

Finally for $M > Q_0$ (and $k_T < k_0$) we use the additive quark model and impulse approximation

$$\sigma_T(\text{AQM}) = \alpha \sum_q \frac{e_q^2}{2\pi} \int dz dk_T^2\, \frac{[z^2+(1-z)^2]k_T^2 + m_q^2}{(\tilde{Q}^2+k_T^2)^2} \times N_c\, \sigma_{q\bar{q}+p}\,(W^2) \tag{37}$$

$$\sigma_L(\text{AQM}) = \alpha \sum_q \frac{e_q^2}{2\pi} \int dz dk_T^2\, \frac{4Q^2\, z^2(1-z)^2}{(\tilde{Q}^2+k_T^2)^2} \times N_c\, \sigma_{q\bar{q}+p}\,(W^2) \tag{38}$$

where for $\sigma_{q\bar{q}+p}$ we take, for the light quarks,

$$\sigma_{q\bar{q}+p}\,(W^2) = \frac{2}{3}\,\sigma_{p\bar{p}}\,(s = \tfrac{3}{2}W^2). \tag{39}$$

The "photon" wave function contains propagators like $1/(\overline{Q}^2 + k_T^2)$ and in impact parameter b_T space it receives contributions from the whole of the b_T plane extending out to infinity. On the other hand confinement restricts the quarks to have limited separation, say $b_T = |\boldsymbol{b}_{1T} - \boldsymbol{b}_{2T}| \lesssim 1$ fm. To allow for this effect we have replaced $\overline{Q}^2$ by $\tilde{Q}^2 = \overline{Q}^2 + \mu^2$ in (37) and (38), where μ is typically the inverse pion radius. We therefore take $\mu^2 = 0.1\text{GeV}^2$. This change has no effect for $Q^2 \gg \mu^2$ but for $Q^2 \lesssim \mu^2$ it gives some suppression of the AQM contribution.

2.4 The quark mass

In the perturbative QCD domain we use the (small) current quark mass m_{curr}, while for the long distance contributions it is more natural to use the constituent quark mass M_0. To provide a smooth transition between these values (in both the AQM and perturbative QCD domains) we take the running mass obtained from a QCD-motivated model of the spontaneous chiral symmetry breaking in the instanton vacuum [20]

$$m_q^2 = M_0^2 \left(\frac{\Lambda^2}{\Lambda^2+2\mu^2}\right)^6 + m_{\text{curr.}}^2. \tag{40}$$

The parameter $\Lambda = 6^{1/3}/\rho = 1.09$ GeV, where $\rho = 1/(0.6\text{ GeV})$ is the typical size of the instanton. μ is the natural scale of the problem, that is $\mu^2 = z(1-z)Q^2 + k_T^2$ or $\mu^2 = z(1-z)Q^2 + (\boldsymbol{l}_T + \boldsymbol{k}_T)^2$ as appropriate. For constituent and current quark masses we take $M_0 = 0.35$ GeV and $m_{\text{curr}} = 0$ for the u and d quarks, and $M_0 = 0.5$ GeV and $m_{\text{curr}} = 0.15$ GeV for the s quarks.

In summary, the q^2 dependence of m_q^2 is obtained from the instanton vacuum model, while the normalisation is fixed by M_0^2. It is interesting to note that this approach gives a value for the quark condensate which is in reasonable agreement with the QCD sum rules originally proposed by Shifman et al.[21]. We will see from Fig. 10 that two very different assumptions for the q^2 dependence of the quark mass do not have a large effect on the behaviour of F_2. Indeed we tried several other forms for the q^2 dependence of m_q^2; all gave similar results to the continuous curves shown in Fig. 10.

3 The description of the data for F_2

Though in principle it would appear that we have a parameter-free[7] prediction of $F_2(x,Q^2)$ at low Q^2, in practise we have to fix the values of the parameters k_0^2 and Q_0^2. Recall that $k_T^2 = k_0^2$ specifies the boundary between the non-perturbative and perturbative QCD components, and that $M^2 = Q_0^2$ specifies the boundary between the VDM and AQM contributions to the non- perturbative component. The results that we present correspond to the choice $Q_0^2 = 1.5$ GeV^2, for which the VDM contribution is computed from the ρ, ω and ϕ meson contributions (with mass $M_V < Q_0$). The more sensitive parameter is k_0^2. We therefore present results for two choices, namely $k_0^2 = 0.2$ and 0.5 GeV^2, which show some interesting and observable differences. The results are much more stable to the increase of k_0^2 from 0.5 to 1 GeV^2.

To calculate the perturbative contributions we need to know the unintegrated gluon distribution $f(x,l_T^2)$, see (22) and (29). To determine $f(x,l_T^2)$ we carry out the full programme described in detail in [14]. We solve a "unified" equation for $f(x,l_T^2)$ which incorporates[8] BFKL and DGLAP evolution on an equal footing, and allows the description of both small and large x data. To be precise we solve a coupled pair of integral equations for the gluon and sea quark distributions, as well as allowing for the effects of valence quarks. As in [14] we take $l_0^2 = 1$ GeV^2, but due to the large anomalous dimension of the gluon the results are quite insensitive to the choice of l_0 in the interval 0.8–1.5 GeV.

The starting distributions for the evolution are specified in terms of three parameters N, λ and β of the gluon

$$xg(x,l_0^2) \;=\; Nx^{-\lambda}(1-x)^{\beta} \tag{41}$$

where $l_0^2 = 1$ GeV^2. At small x the gluon drives the sea quark distribution. The k_T factorization theorem gives

$$S_q(x,Q^2) = \int_x^1 \frac{dz}{z} \int \frac{dk^2}{k^2}\, S^q_{\rm box}(z,k^2,Q^2) \times f\left(\frac{x}{z},k^2\right) \tag{42}$$

where $S_{\rm box}$ describes the quark box (and crossed box) contribution. The full expression for $S_{\rm box}$ is given in [14]. Thus the sea S_q is given in terms of the gluon f except for the contribution from the non-perturbative region $k^2 < k_0^2$, where we take

$$S_u^{\rm np} \;=\; S_d^{\rm np} \;=\; 2S_s^{\rm np} \;=\; C\,x^{-0.08}(1-x)^8. \tag{43}$$

[7] Apart of course from the form of the input gluon distribution, $g(x,l_0^2)$

[8] Following [14] we appropriately constrain the transverse momenta of the emitted gluons along the BFKL ladder. There is an indication, from comparing the size of the next-to-leading $\ln(1/x)$ contribution [22] to the BFKL intercept with the effect due to the kinematic constraint [23], that the incorporation of the constraint into the evolution analysis gives a major part of the subleading $\ln(1/x)$ corrections

Table 1. The values of the gluon parameters of (41)

	k_0^2 (GeV^2)	N	λ	β	χ^2/datapoint [423 points]
Fit A	0.2	0.97	0.16	3.6	1.09
Fit B	0.5	0.42	0.32	3.7	1.70

The parameter C is fixed by the momentum sum rule in terms of the parameters N, λ and β specifying the gluon. The charm component of the sea is obtained entirely from perturbative QCD (see [14]) with the charm mass $m_c = 1.4$ GeV. The valence quark contribution plays a very minor role in our analysis and so we take it from the GRV set[9] of partons [24]. Of course the sea quark distributions $S_q(x,Q^2)$ of (42) (and (43)) are used only to get a more precise determination of $f(x,l_T^2)$ through the coupled evolution equations. These values for S_q are not used in our fit to the F_2 data since essentially the same form of the sea contribution is already embedded in (22) and (29).

We determine the parameters N, λ and β by fitting to the available data for F_2 with $x < 0.05$. We present two fits corresponding to a larger perturbative QCD contribution (Fit A with $k_0^2 = 0.2$ GeV^2) and a smaller pQCD component (Fit B with $k_0^2 = 0.5$ GeV^2). The values of the gluon parameters are given in Table 1 and the quality of the description of the F_2 data is shown in Fig. 4. Only a selection of the data fitted are shown in Fig. 4. Both descriptions are in general satisfactory, but Fit A is superior mainly due to Fit B lying below the data for $Q^2 \simeq 1$ GeV^2. This difference is better seen in Fig. 5 which shows the fit as a function of Q^2 for various fixed values of x. We see that Fit A, with the larger perturbative component is more able to accommodate the charge in slope going from high to low Q^2. It is informative to show the components of the cross section. The breakdown is shown in Figs. 6 and 7 for Fits A and B respectively for the maximum energy $W = 245$ GeV for which data are available. It appears that the low Q^2 behaviour of the pQCD component with low l_T plays the vital role.

The description of the F_2 data by Fit A is better than that obtained by Badelek and Kwiecinski [4], which is to be expected since we perform a fit to the data, albeit with a very economical parametrization. Figure 5 also shows the HERA photoproduction measurements at $W = 170$ and 210 GeV. These data are not included in the fit. We see that our description overshoots the published H1 [26] and ZEUS [27] measurements, although by a smaller margin than that of [4]. On the other hand our extrapolation is in excellent agreement with a subsequent analysis of ZEUS data performed in [28]. We will return to the comparison with photoproduction data when we study the effects of a different choice of the quark mass.

[9] The GRV valence distributions were fitted to the MRS(A) distributions [25] at $Q^2 = 4$ GeV^2

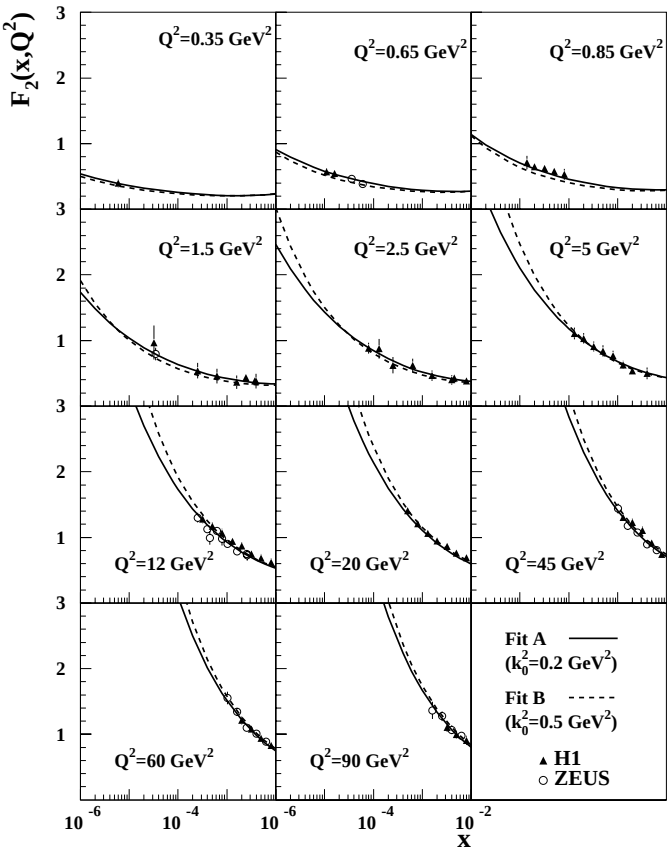

Fig. 4. The description of the F_2 data obtained in Fits A and B. Only a subset of the data fitted is shown

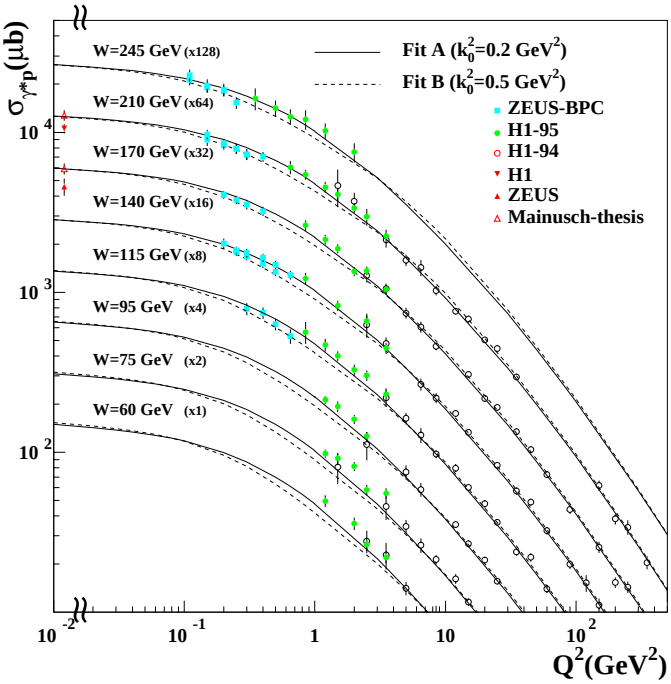

Fig. 5. The curves are the values of the virtual photon-proton cross section $\sigma_{\gamma^* p}$ of (5) as a function of Q^2 for various values of the energy $W = \sqrt{s}$ corresponding to Fits A and B (multiplied by the factor shown in brackets). The data [1,2] are assigned to the value of W which is closest to the experimental W bin. The upper, lower photoproduction (solid triangular) data points correspond to $W = 210$, 170 GeV and are from the H1 [26] and ZEUS [27] collaborations respectively. The open triangular points are obtained from an analysis of ZEUS photoproduction data reported in a thesis by Mainusch [28]

4 Discussion

We have made what appears to be in principle a prediction of F_2, or rather of $\sigma_{\gamma^* p}$, over the entire Q^2 range which relies only on the form of the initial gluon distribution, see (41) and the parameter values of Table 1. However a comparison of the results of Fits A and B show that in practice the results are dependent on the choice of the boundary $k_T^2 = k_0^2$ between the perturbative and non-perturbative contributions, where $\pm \boldsymbol{k}_T$ are the transverse momenta of the incoming q and $\bar{q}$ which result from the $\gamma^* \to q\bar{q}$ transition.

There are compelling reasons to select Fit A with $k_0^2 = 0.2$ GeV^2, which has the larger perturbative QCD contribution. Fit A is not only preferred by the data, but it also yields an input gluon with a more reasonable small x behaviour. In fact for Fit A ($k_0^2 = 0.2$ GeV^2) the AQM contribution is almost negligible and the fit produces a reasonable λ, namely $\lambda = 0.16$. On the other hand Fit B (with $k_0^2 = 0.5$ GeV^2) requires a larger λ, $\lambda = 0.32$, in order to compensate for the much more flat $x^{-0.08}$ behaviour of the rather large AQM component. Further support for Fit A comes from the predictions for the longitudinal structure function, F_L. Figure 8 shows that the prediction from Fit B is much larger than that of Fit A due mainly to the large AQM contribution. Figure 8 also shows the expectations for F_L from the analysis of [29] and from the MRST partons [30] of the most recent global parton analysis. We see these independent determinations of F_L favour the prediction of Fit A.

For completeness we show by the dashed curve in Fig. 9 the predictions of σ_L/σ_T versus Q^2 obtained from Fit A. This figure also shows the effect of replacing (32) by (33) in the formula for the VDM contribution to F_L. Recall that (33) was motivated by the possibility that the ratio $\sigma_L(\rho)/\sigma_L(\rho)$ for ρ meson electroproduction tends to a constant value A as $Q^2 \to \infty$. We see from Fig. 9 that this change to the VDM contribution affects F_L, and hence σ_L/σ_T, mainly in the interval $0.2 < Q^2 < 10$ GeV^2. It is straightforward to deduce from Fig. 9 the effect of changing the value of the parameter ξ_0 of (33) to match the constant limit A observed for the ρ ratio.

A remarkable feature of the recent measurements [1, 2] of $\sigma(\gamma^* p) = (4\pi^2\alpha/Q^2)\, F_2(x, Q^2)$ at fixed W, is the transition from a flat behaviour in the low Q^2 domain to the steep $\sim Q^{-2}$ fall off characteristic of perturbative QCD, see Fig. 5. The transition appears to occur at $Q^2 \sim 0.2$GeV^2. Such a break with decreasing Q^2 may reflect either the saturation due to the onset of absorption

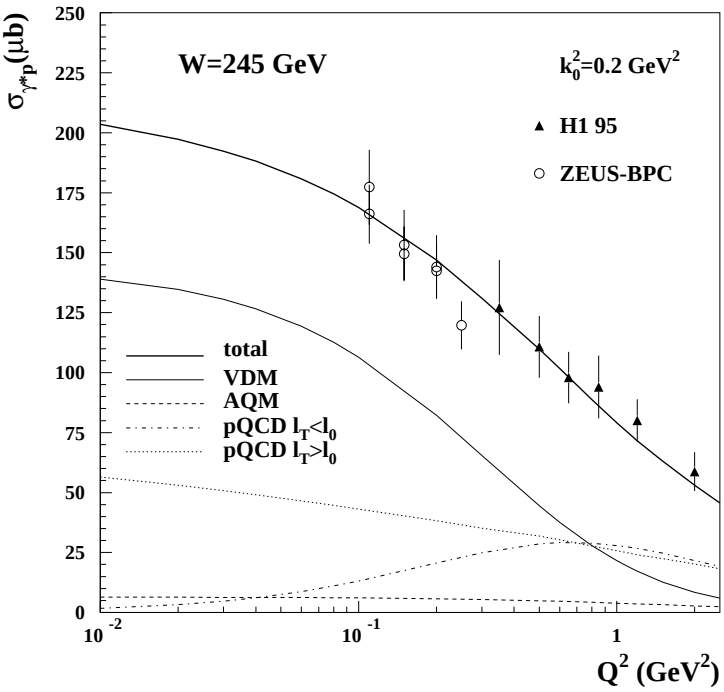

Fig. 6. The various components of $\sigma_{\gamma^* p}$ (as defined in Sect. 2.3) shown as a function of Q^2 at $W = 245$ GeV for Fit A (with $k_0^2 = 0.2$ GeV^2). The bold curve shows their sum, $\sigma_{\gamma^* p}$, compared to the HERA measurements

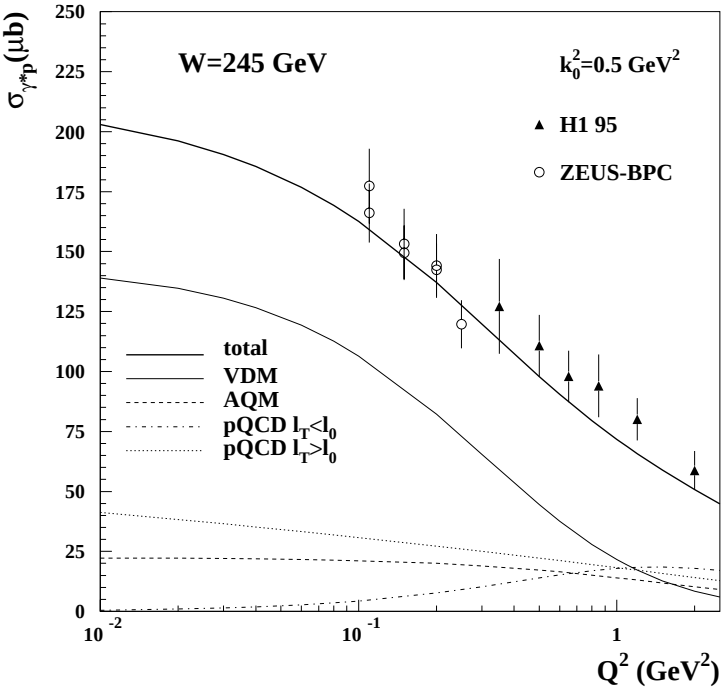

Fig. 7. The same as Fig. 6 but for Fit B (with $k_0^2 = 0.5$ GeV^2). The poorer description of the data in the region $Q^2 \sim 1$ GeV^2, as compared to Fit A, is clearly apparent and can be attributed to the smaller perturbative QCD component at low gluon l_T

corrections or the fact that we are entering the confinement domain. The observed features of the data favour the last possibility, which we allow for through the parameter μ which we introduce below (39). First there is no similar break in the behaviour of F_2 as a function of x at low x which would be expected if absorptive corrections were important. A related observation is that the break, as a function of Q^2, appears to occur at the same value $Q^2 \sim 0.2$GeV^2 for those W values for which data are available. Moreover we directly estimated the effect of the absorptive corrections in the perturbative QCD component[10] using the eikonal rescattering model and found

[10] In our approach the main effect of screening is hidden by the fact that we effectively take an $x^{-0.08}$ behaviour of the "soft" (VDM + AQM) contribution

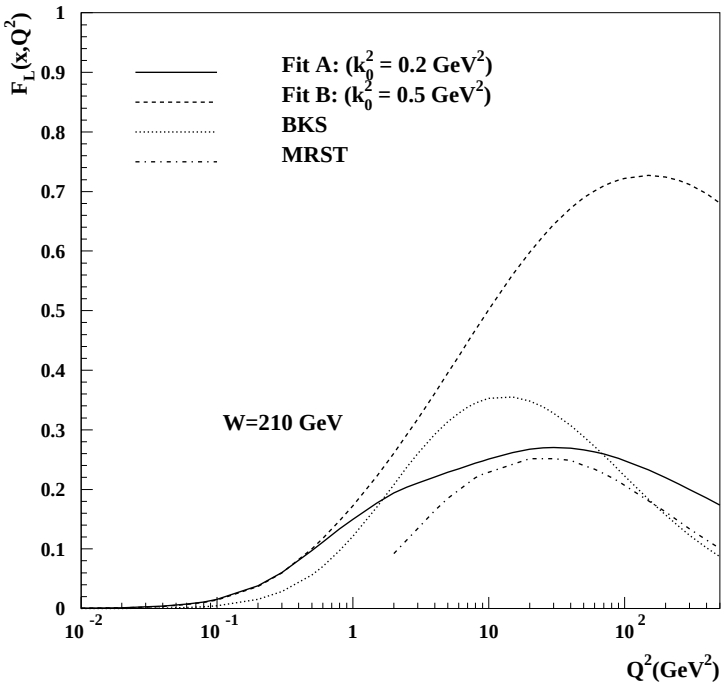

Fig. 8. The predictions for F_L versus Q^2 at $W = 210$ GeV from Fits A, B (with $k_0^2 = 0.2$ and 0.5 GeV^2 respectively), together with the values obtained by Badelek, Kwiecinski and Stasto [29] and from the MRST set of partons [30]

that they give a negligibly small effect on the Q^2 behaviour of the cross section and of F_2. On the other hand, if the break is due to confinement then it is expected to occur at a value of $\overline{Q}^2$ which corresponds to the distances of the order of 1 fm, that is

$$z(1-z)\,Q^2 \;\sim\; Q^2/5 \;\sim\; (0.2\text{GeV})^2 \qquad (44)$$

which gives $Q^2 \sim 0.2\text{GeV}^2$ where the break is observed.

In our calculations we have used a running quark mass which links the current ($m_{\rm curr}$) to the constituent (M_0) mass. The growth of m_q in the transition region from perturbative QCD to the large distance domain is an important non-perturbative effect, which we find is required by the F_2 data. From the theoretical point of view such a behaviour of m_q may be generated by the spontaneous breakdown of chiral symmetry in the instanton QCD vacuum [20]. The qualitative features are that $m_q \sim M_0$ if the virtuality q^2 of the quark is less or of the order of the square of the inverse of the instanton size, but that m_q decreases quickly as q^2 increases. In our analysis we have used a simplified power approximation for m_q, see (40).

It is interesting to explore the effect of a different choice of quark mass. The dashed curves in Fig. 10 show the effect of using the constituent (fixed) mass M_0 of the quarks in all the contributions to F_2 or $\sigma(\gamma^* p)$. As expected in the large $Q^2 \gg M_0^2$ perturbative domain the change has little effect. For small Q^2 it reduces the predictions. For example, the photoproduction estimates for $W \sim 200$ GeV are reduced by more than 10% and would bring our analysis more into line with the published H1 and ZEUS photoproduction measurements. However our running quark mass predictions (continuous curves) are more physically motivated and should be more reliable. It will be interesting to see if their agreement with the experimental values extracted in [28] is maintained when the new photoproduction measurements are available from the HERA experiments.

A noteworthy point of our description of the F_2 data is the importance of the non-diagonal ($M \neq M'$) perturbative QCD contribution to the double dispersion relation (1). The contribution, which comes from the interference terms in (22) (and (29)), corresponds to the diagram shown in Fig. 3. It clearly has a negative sign, and moreover

$$\left\{M^2 = \frac{k_T^2 + m_q^2}{z(1-z)}\right\} \neq \left\{M'^2 = \frac{(\boldsymbol{k}_T + \boldsymbol{l}_T)^2 + m_q^2}{z(1-z)}\right\}. \qquad (45)$$

After the integration over the azimuthal angle in (22), the interference term exactly cancels the diagonal first term for any $l_T < k_T$ in the limit of $Q^2 \to 0$ and $m_q = 0$. As a result the perturbative component of the cross section coming from the region of small l_T essentially vanishes[11] as $Q^2 \to 0$. This property, seen in the $l_T < l_0$ components shown in Figs. 6 and 7, helps to reproduce the very flat Q^2 behaviour of $\sigma(\gamma^* p)$ observed at low Q^2, $Q^2 \lesssim 0.2\text{GeV}^2$. In fact we cannot achieve a satisfactory description of the F_2 data in the transition region and below without this cancellation. Thus the fact that the low l_T gluon contribution becomes very small as Q^2 decreases (and in fact vanishes for $l_T < k_T$ in the $Q^2 \to 0$ limit) may be considered as a justification of the perturbative QCD contribution to F_2 for low Q^2. The VDM cross section (and other diagonal contributions as well) decrease as $1/(M_V^2 + Q^2)^2$

[11] Of course there is also a non-negligible contribution coming from the domain $l_T > k_T$ which does not vanish as $Q^2 \to 0$

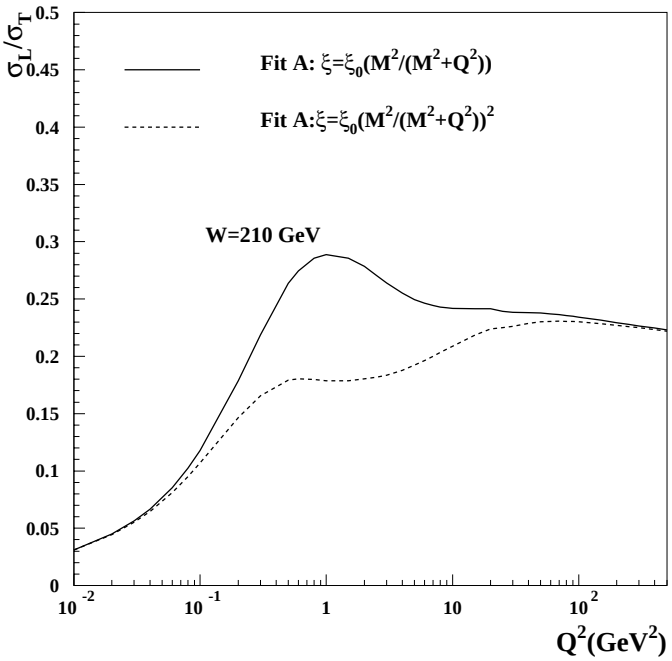

Fig. 9. The dashed curve is the prediction for σ_L/σ_T versus Q^2 at $W = 210$ GeV from Fit A. For comparison the continuous curve is the prediction obtained using a different choice of the VDM contribution to F_L; namely using (33) in the place of (32)

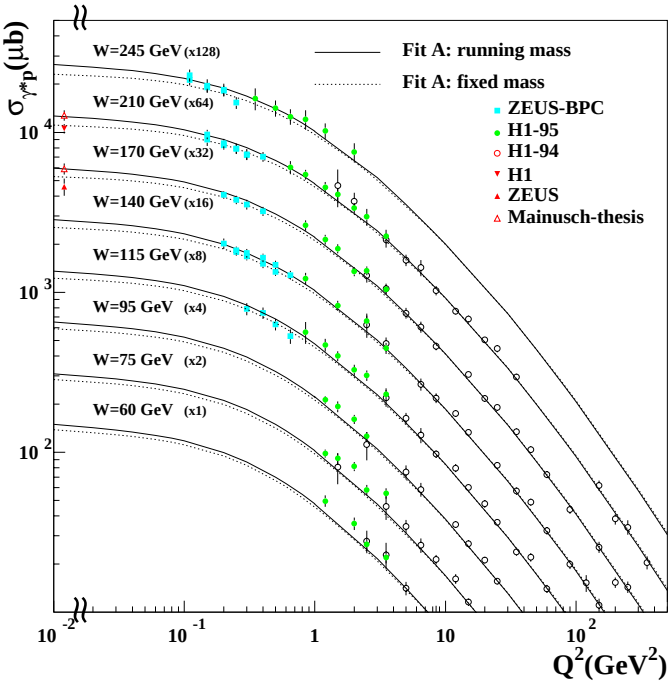

Fig. 10. The dotted curves show the effect of using a (fixed) constituent mass, M_0, in all contributions. The running mass fit (continuous curves) and the data are those of Fig. 5

so we require just such a component which increases with Q^2 in order to compensate the decrease of the diagonal terms. The compensation is well illustrated by Figs. 6 and 7 which show the behaviour of the various components as a function of Q^2. Of course the compensation (that is the effect of the vanishing of the low l_T^2 contribution as $Q^2 \to 0$) is more manifest in the Fit A where a larger part of the phase space is described in terms of perturbative QCD.

It is interesting to note that in this paper we have included two different types of interference effect. First we have the dominant interference between the large M and M' states which gives rise to the decrease of the pure perturbative small l_T component of the cross section as $Q^2 \to 0$, and which is responsible for the good description of the low Q^2 data. Then there is the interference between the perturbative and non-perturbative amplitudes which we have modelled using the perturbative formula in the region of small M' and/or small $|\boldsymbol{k}_T + \boldsymbol{l}_T|$. We have noted that this contribution is small due to the infrared stability of the integral, as was shown in (26).

In summary we obtain an excellent description of F_2, or rather of $\sigma_{\gamma^* p}$, over the entire Q^2 range (from very low to high values of Q^2) in terms of physically motivated perturbative and non-perturbative contributions.We list some distinctive features of our approach below.

1. Our treatment of the perturbative region is state-of-the-art. We repeat, and extend, the entire numerical analysis of [14]. In this way we are able to work directly in terms of the unintegrated gluon distribution, which is determined by solving coupled integro-differential equations that embody both DGLAP and BFKL evolution. These unified equations are applicable over the entire perturbative region. This is a distinct advantage over other treatments. Remarkably few parameters are required to fully specify the perturbative component.
2. We make a careful treatment of the non-perturbative regime. We use the VDM where it is well-established and for higher masses we use reliable input. No free parameters are introduced. However the results are sensitive to the value of k_0^2 which separates the perturbative from the non-perturbative domain.
3. We emphasize the importance of the perturbative contribution in the non-perturbative domain. In particular we find that non-diagonal ($M \neq M'$) perturbative QCD contributions play an important role. They cancel the diagonal contributions for $l_T < k_T$ as Q^2 tends to zero. This novel and interesting effect turns out to be required to describe the behaviour of F_2 at low Q^2. Indeed in our physically constrained approach, with very few parameters, we are unable to describe the data in the transition region (and below) without this cancellation.
4. The choice of the boundary between the perturbative and non-perturbative domains which gives an excellent fit to the data, is also found to yield a physically sensible gluon distribution and reasonable predictions for F_L.

Acknowledgements. We thank Krzysztof Golec-Biernat, Jan Kwiecinski and Vladimir Shekelyan for valuable discussions and their interest in this work. MGR thanks the Royal Society, INTAS (95-311) and the Russian Fund of Fundamental Research (98 02 17629), for support. AMS thanks the Polish State Committee for Scientific Research (KBN) grants No. 2 P03B 089 13 and 2 P03B 137 14 for support. Also this work was supported in part by the EU Fourth Framework Programme 'Training and Mobility of Researchers', Network 'Quantum Chromodynamics and the Deep Structure of Elementary Particles', contract FMRX-CT98-0194 (DG 12 - MIHT).

References

1. H1 collaboration: C. Adloff et al., Nucl. Phys. B **497**, 3 (1997); H1 collaboration: S. Aid et al., Nucl. Phys. B **470**, 3 (1996)
2. ZEUS collaboration: J. Breitweg et al., Phys. Lett. B **407**, 432 (1997)
3. V.N. Gribov, Sov. Phys. JETP **30** 709 (1970); J.J. Sakurai, D. Schildknecht, Phys. Lett. **40B** 121 (1972); B. Gorczyca, D. Schildknecht, Phys. Lett. **47B** 71 (1973)
4. B. Badelek, J. Kwiecinski, Phys. Lett. B **295**, 263 (1992)
5. A.M. Cooper-Sarkar, R.C.E. Devenish, A. De Roeck, Int. J. Mod. Phys. A **13**, 3385 (1998)
6. D. Schildknecht, H. Spiesberger, Bielefeld `BI-TP 97/25, hep-ph/9707447` (preprint); D. Schildknecht, Acta Phys. Pol. B **28**, 2453 (1997)
7. G. Kerley, G. Shaw, Phys. Rev. D **56**, 7291 (1997)
8. K. Adel, F. Barreiro, F.J. Yndurain, Nucl. Phys. B **495**, 221 (1997); K. Adel, F.J. Yndurain, FTUAM-96-44, `hep-ph/9612469`
9. A. Capella, A. Kaidalov, C. Merino, J. Tran Thanh Van, Phys. Lett. B **337**, 358 (1994)
10. H. Abramowicz, E.M. Levin, A. Levy, U. Maor, Phys. Lett. B **269**, 465 (1991)
11. K.J. Golec-Biernat, M. Wusthoff, Durham DTP/98/50, `hep-ph/9807513` (preprint)
12. H. Abramowicz, A. Levy, DESY preprint-97-251 (1997)
13. E. Gotsman, E.M. Levin, U. Maor, Eur. Phys. J. C **5**, 303 (1998)
14. J. Kwiecinski, A.D. Martin, A.M. Stasto, Phys. Rev. **D56** 3991 (1997); J. Kwiecinski, A.D. Martin, A.M. Stasto, Acta Phys. Polon. B **28**, (12) 2577 (1997)
15. E.M. Levin, A.D. Martin, M.G. Ryskin, T. Teubner, Z. Phys. C **74**, 671 (1997)
16. A.H. Mueller, Nucl. Phys. B **335**, (1990) 115; S. Brodsky, P. Lepage, Phys. Rev. D **22**, (1980) 2157.
17. N.N. Nikolaev, B.G. Zakharov, Z. Phys. C **49**, 607 (1991)
18. T.H. Bauer, R.D. Spital, D.R. Yennie, F.M. Pipkin, Rev. Mod. Phys. **50** 261 (1978)
19. ZEUS collaboration: contribution to the 6th International Workshop on *Deep Inelastic Scattering and QCD* (DIS98), Brussels, April 1998
20. V.Yu. Petrov et al., Phys. Rev. D **57** 4325 (1998)
21. M. Shifman, A. Vainshtein, V. Zakharov, Nucl. Phys. B **147** 385,488,519 (1979)
22. V.S. Fadin, L.N. Lipatov, Phys. Lett. **B429** 127 (1998); see also V.S. Fadin, L.N. Lipatov, contribution to DIS 98, Brussels, April 1998; G. Camici, M. Ciafaloni, contribution to DIS 98, Brussels, April 1998
23. J. Kwiecinski, A.D. Martin, P.J. Sutton, Z. Phys. C **71**, 585 (1996)
24. M. Glück, E. Reya, A. Vogt, Z. Phys. C **67**, 433 (1995)
25. A.D. Martin, R.G. Roberts, W.J. Stirling, Phys. Rev. D **50** 6734 (1994)
26. H1 collaboration: S. Aid et al., Z. Phys. C **69**, 27 (1995)
27. ZEUS collaboration: M. Derrick et al., Z. Phys. C **63**, 408 (1994)
28. J. Mainusch, *Measurement of the total photon-proton cross section at HERA energies, University of Hamburg*, Ph.D. thesis, DESY F35D-95-14, 1995
29. B. Badelek, J. Kwiecinski, A. Stasto, Z. Phys. C **74**, 297 (1997); A. Stasto, Acta Phys. Polon. B **27**, 1353 (1996)
30. A.D. Martin, R.G. Roberts, W.J. Stirling, R.S. Thorne, Eur. Phys. J. C **4**, 463 (1998)